INSTITUTE OF PHYSICS PUBLISHING NANOTECHNOLOGY
Nanotechnology **17** (2006) 1160–1165 doi:10.1088/0957-4484/17/4/053

Nanopatterned self-assembled monolayers

Gabriel G Baralia, Antoine Pallandre[1], Bernard Nysten and Alain M Jonas[2]

Unité de Physique et de Chimie des Hauts Polymères (POLY) and Research Center on Micro- and Nanoscopic Materials and Electronic Devices (CeRMiN), Université Catholique de Louvain, Place Croix du Sud, 1, B-1348 Louvain-la-Neuve, Belgium

E-mail: alain.jonas@uclouvain.be

Received 13 September 2005, in final form 14 December 2005
Published 2 February 2006
Online at stacks.iop.org/Nano/17/1160

Abstract
We report on the fabrication of chemically nanopatterned gold surfaces by combining electron-beam lithography with gas and liquid phase thiolization. The line-edge roughness of the patterns is ∼4 nm, corresponding to a limiting feature size in the range of 15 nm. Indications for a lower packing density of the self-assembled monolayers grown in the nanofeatures are given, and evidences for the bleeding of thiols along the grain boundaries of the gold substrate are displayed. A comparison is provided between nanopatterned thiol and silane monolayers on gold and on silicon wafers, respectively. The line-edge roughnesses are shown to be close to each other for these two systems, indicating that the limiting step is currently the lithography step, suggesting possible improvement of the resolution. The advantages and drawbacks of thiol versus silane monolayers are finally discussed with respect to the formation of chemically nanopatterned surfaces.
M Supplementary data files are available from stacks.iop.org/Nano/17/1160

1. Introduction

Electron-beam lithography (EBL) is an important current technique for the fabrication of nanodevices. Given its extensive use in the field of inorganic semiconductor technology, it has reached a high degree of maturity, and combines a number of attractive features, such as a high resolution [1] and the possibility of patterning large areas with virtually any shape. Even when using conventional organic resists such as poly(methyl methacrylate) (PMMA), the limit of resolution of EBL can be pushed down to well below 10 nm, using appropriate development sequences [2, 3]. Therefore, it is tempting to transpose its advantages to other systems of interest such as soft-condensed materials. Recently, we have shown how to combine electron-beam lithography with silanation reactions to produce binary chemically nanopatterned silicon surfaces [4], which were then used to spatially direct macromolecular adsorption processes such as layer-by-layer assembly [4, 5] or protein adsorption [6]. Stamou *et al* have subsequently reported on a similar methodology to produce nanopatterned gold surfaces by replacing silanes with thiols [7]. Here, we extend this previous work to a wider range of thiols, and provide a comparison of the two patterning methods, silanes on silicon on the one hand, and thiols on gold surfaces on the other hand.

Thiol monolayers on gold surfaces have already been extensively used for nanofabrication purposes [8], because they easily form well-ordered and densely packed self-assembled monolayers (SAMs) by adsorption from the liquid or gas phases, offering a broad variety of end groups to control and tailor surface properties [9]. *Micrometre*-scale patterns of thiol SAMs are conveniently produced by the stamping technique developed by Whitesides and co-workers [10], or by methods derived from it [11]. However, the down-scaling of this method to the *nanometre* scale proves to be difficult, and alternative methodologies were thus proposed for this range of sizes. For instance, tips of atomic force microscopes are used to modify locally pre-formed SAMs [12], or to transfer locally a thiol ink on a bare gold surface such as in dip-pen nanolithography [13]. Such atomic force microscope based methods are of high resolution and limited cost, but frequently suffer from limited throughput. Other patterning methods of thiol-based SAMs rely on the local irradiation of a pre-formed SAM by photons, ions or electrons [14–16], providing high resolution in specific instances but more limited chemical versatility. In the present

[1] Present address: Unité de Physico-Chimie, Institut Curie, 11 rue Pierre et Marie Curie, 75 005 Paris, France.
[2] Author to whom any correspondence should be addressed.

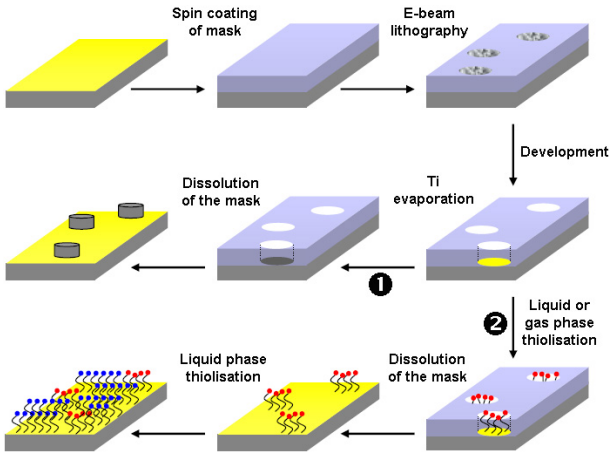

Figure 1. Schematic presentation of the route used to create 2D chemically nanopatterned substrates (route 2). The quality of the electron-beam lithography was checked by Ti lift-off (route 1). (This figure is in colour only in the electronic version)

work, we used EBL to define openings in a PMMA mask spin-coated onto gold (figure 1). Thiols were then deposited on the exposed gold surface. After subsequent removal of the PMMA mask, a background thiol was deposited over the rest of the surface. Compared with previously reported methods, our procedure combines the high resolution afforded by EBL with the chemical versatility of thiol SAMs.

2. Experimental section

2.1. Fabrication of nanopatterned gold surfaces

Template-stripped gold (TSG) surfaces were prepared as described previously [17]. After preparation, the TSG surfaces were covered by a 95–100 nm spin-coated resist layer (anionic PMMA resist, $M_n = 142\,000$ g mol^{-1}, $M_w = 160\,000$ g mol^{-1}, obtained from Polymer Source, ref. P1409), dissolved into toluene (HPLC grade, Acros, 20 g ml^{-1}) and annealed at 170 °C for 12 h. Nanoscopic features (lines, dots, squares, circles) were drawn over the surface by electron-beam lithography (EBL). EBL was performed with a XL 30S Philips scanning electron microscope (field emission gun) associated with an Elphy Plus lithographic system. The development of the exposed regions was performed with a mixture of isopropanol (HPLC grade, Acros) and methyl isobutylketone (analytical grade, Carlo Erba) (1:3 v/v) for 90 s. The samples were then rinsed in isopropanol for 30 s and in ultra-pure water for several minutes. Two samples were always prepared identically; one of them was used for the preparation of the 2D chemical nanopatterns and the other one to check the quality of the lithography, using a 10 nm titanium lift-off (figure 1, route 1). Electron-beam nanolithographed TSG substrates were then placed for 1 h in an argon-filled temperature-controlled reactor containing a thiol in the vapour phase at 70 °C (11-mercapto-1-undecanol (95%, Aldrich) or dodecanethiol (98%, Acros)) (route 2, figure 1), or immersed for more than 18 h in a 2 mM solution of octadecylmercaptan (98%, Aldrich) in spectroscopy grade ethanol (Merck). Gas-phase thiolization was preferred for very small feature sizes (less than 50 nm) to avoid problems that can appear due to capillarity, or swelling of the epoxy glue which supports the ultra-flat gold substrates [17]. After removal from the reactor or from the thiol solution, the samples were rinsed with pure ethanol and blown dry with pure argon; subsequently, the PMMA mask was removed by flushing the surface with hot dichloromethane (HPLC grade, Acros). After removal of the mask, the samples were immersed into a 2 mM solution of a second thiol (dodecanethiol (98%, Acros) or 11-mercapto-1-undecanol (95%, Aldrich)) in spectroscopy grade ethanol for 2 h at 5 °C to form the background, thereby producing a 2D chemically pattern (figure 1, route 2). The second thiolization was performed from the liquid phase at 5 °C for 2 h only, in order to limit the exchange between thiol species as detailed elsewhere [18, 19].

2.2. Fabrication of nanopatterned silicon surfaces

Such surfaces were prepared as reported previously [4], using a method similar to route 2 in figure 1 with silanes and silicon replacing thiols and gold, respectively.

2.3. Characterization of the nanopatterned surfaces by atomic force microscopy (AFM)

Atomic force microscopy (topography, and lateral force, LFM) images were recorded in air on two types of samples: samples after only one deposition of thiol in the liquid phase, followed by removal of the mask; and samples functionalized by two thiols (2D chemical nanopatterns). The AFM experiments were conducted with an Autoprobe CP (Thermomicroscopes, Sunnyvale, CA), a PicoSPM (Molecular Imaging, Phoenix, AZ) controlled by a Nanoscope III electronics (Digital Instruments, Santa Barbara, CA) or a Nanoscope IV (Digital Instruments, Santa Barbara, CA). Cantilevers were silicon Ultralevers (Thermomicroscopes) with a spring constant of about 0.25 N m^{-1} and an integrated Si tip with a typical radius of curvature of 10 nm. A second-order flattening procedure (line by line) was performed on all the AFM images.

Forward and backward AFM–LFM images were added to obtain a so-called 'slope' image, and subtracted to get a friction image, using procedures detailed previously [19]. For our samples of very limited roughness, the 'slope' image can be considered to approximate the variation of the topography of the sample. The nanofeatures were analysed with built-in and home-made routines running under Igor Pro (Wavemetrics, Lake Oswego, OR). The images were first discriminated with a thresholding operation to produce black and white images. Then, the contours of the nanofeatures were delineated, and average objects of identical area and centre-of-mass were superimposed on these features. The line-edge roughness σ, which is the roughness of the actual contours of the nanofeatures, was computed as the root-mean-square (rms) average distance between the actual contours of the nanofeatures and the contours of the average objects.

3. Results and discussion

To limit intricacies related to the large intrinsic roughness of evaporated gold films, we used template-stripped gold

(TSG) surfaces as substrates [17]. The quality of the EBL on the TSG was first verified by Ti lift-off (figure 1, route 1), which consists in the evaporation of 10 nm of Ti into the nanoscopic holes created by EBL followed by dissolution of the mask [20]. Typical images of Ti lift-offs on TSG are presented in the supplementary information available at stacks.iop.org/Nano/17/1160. No visible differences could be found between lithographed features on Si or TSG, showing the versatility of EBL with respect to the nature of the substrate. To check the possibility of the self-assembly of thiols in the nanoholes defined by lithography, images of the substrates were obtained by atomic force microscopy in topography and lateral force after the first thiolization and removal of the PMMA mask, i.e., before the application of the second, background thiol. Figure 2 presents a set of AFM images of octadecylmercaptan lines of about 80 nm width deposited from the liquid phase into nanotrenches of linear shape. Figures 2(a) and (b) are lateral force mode (LFM) images recorded for two different scan directions. The reversal of the contrast upon reversing the scan direction testifies to the chemical origin of the contrast. The subtraction of these two images provides the friction image shown in figure 2(d) which, as expected, indicates a higher friction of the atomic force microscope's tip on the bare gold surface as compared to the octadecylthiol lines. The addition of the two LFM images results in the 'slope' image of figure 2(c), which concentrates the topographical information present in the LFM images. Although noisy, the 'slope' image indicates that thiol lines protrude over the substrate. This is fully confirmed by the topographic AFM image shown in figure 2(e). Due to the strong topographical contrast arising from the presence of grain boundaries and terraces on the gold surface, the topography of the thiol lines appears only weakly in the topography image, but is evidenced in the height profile displayed in figure 2(f). An average value of 1.3 ± 0.1 nm was found for the height of the thiol lines. This value is relatively close to the expected theoretical thickness of an SAM of octadecylmercaptan molecules, assuming a chain tilt angle of $\sim 30°$ [21], but is significantly smaller than reported experimental values for a homogeneous monolayer (2.2–2.6 nm) [22], suggesting that the patterned SAM is of lower packing quality. Decreased packing may originate from molecular pits or from a low grafting density, resulting in gauche defects or other conformational distortions of the chains which partially collapse on the substrate. This results in a lower layer thickness and also in higher friction in the LFM, due to the increased number of available vibrational and relaxation modes under contact, which increases energy dissipation [24, 25]. It is well known that high temperatures or even simple immersion in various solvents may lead to desorption of thiols [19, 33]. Since the samples are flashed with hot dichloromethane to remove the PMMA mask after the first thiolization, this could be a first reason explaining the limited packing density of the thiol monolayer. Other possibilities to explain the lower packing density are the confinement of the thiol monolayer to features as small as 30 nm, which prevents the system from forming 2D crystals of large size, and the use of TSG surfaces, which are polycrystalline and exhibit many discontinuities [17]. This would favour liquid-like structures and more visco-elastic monolayers inside the

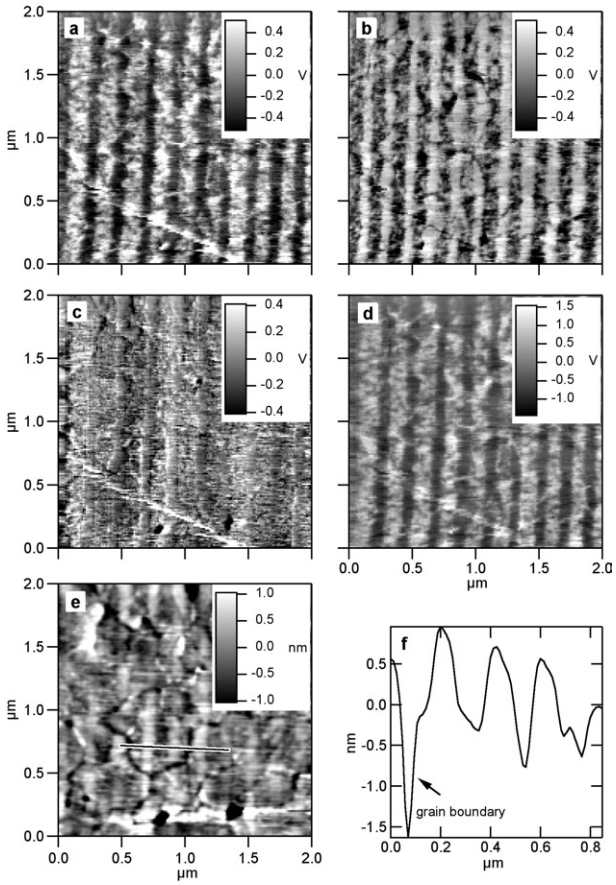

Figure 2. AFM images of octadecylmercaptan lines of 80 nm width deposited from the liquid phase through the trenches of a PMMA mask, after mask removal. ((a), (b)) Trace and retrace LFM images, (c) 'slope' image resulting from the addition of the two LFM images, (d) friction image resulting from the subtraction of the two LFM images, (e) corresponding AFM topographic image, (f) height profile along the line displayed in part (e).

nanozones, which would also interact more strongly with the tip due to enhanced contact area, compared to highly crystalline regions. This set of images also illustrates the superiority of the AFM lateral force mode compared to the topographical mode when attempting to visualize flat chemical nanopatterns. Therefore, in what follows, we will concentrate on LFM images.

Binary nanopatterned surfaces were obtained by applying a second thiolization from the liquid phase at low temperature, after a first thiolization from the gas phase through the holes of the PMMA mask, and mask removal (figure 1, route 2). Figure 3 presents a set of LFM images, where the nanofeatures consist of 11-mercapto-1-undecanol (−OH-ended) SAM lines surrounded by a dodecanethiol ($-CH_3$-ended) background. By contrast, figure 4 presents images where the CH_3-ended thiol was first deposited from the gas phase in nanoholes of circular shape, before applying a background of 11-mercapto-1-undecanol. Because such thiols are of identical chain length, the topographical AFM images were found to be virtually featureless, except for the presence of gold grain boundaries. This is also confirmed by the 'slope' images obtained by adding the LFM images (figures 3 and 4(c)). However, the

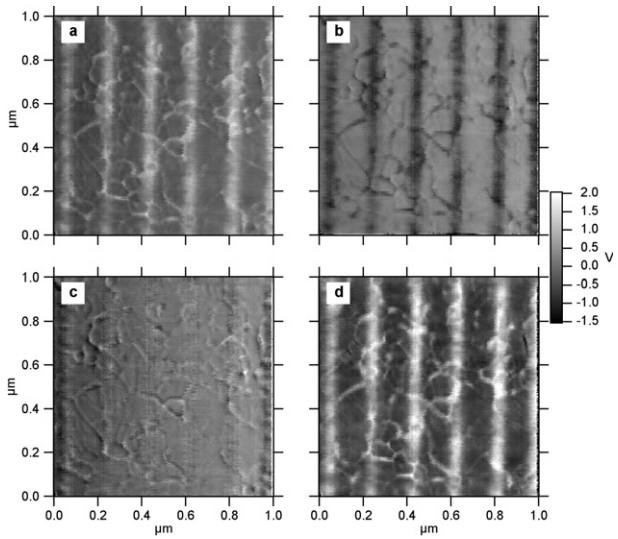

Figure 3. LFM images of a nanopatterned thiol SAM, showing the bleeding of the first thiol deposited along gold grain boundaries. The nanofeatures consist of 11-mercapto-1-undecanol lines of 50 nm average width, in a background of dodecanethiol. ((a), (b)) Trace and retrace LFM images, (c) 'slope' image resulting from the addition of the two LFM images, (d) friction image resulting from the subtraction of the two LFM images.

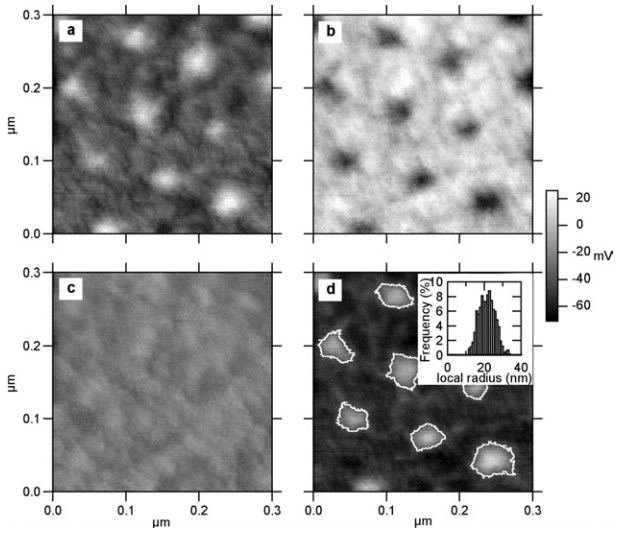

Figure 4. LFM images of a nanopatterned thiol SAM, where the nanofeatures consist of dodecanethiol dots of 40 nm average diameter, in a background of 11-mercapto-1-undecanol. ((a), (b)) Trace and retrace LFM images, (c) 'slope' image resulting from the addition of the two LFM images, (d) friction image resulting from the subtraction of the two LFM images. The white contour lines indicate the edges of the two chemical domains, and were used to compute the line-edge roughness, σ. The inset in (d) is the distribution of local radius.

friction images confirm the success of the patterning, although some grain boundaries of gold are found to be decorated by the first deposited thiol (figure 3), indicating that these thiols crept along the grain boundaries during their deposition. This phenomenon was not observed so prominently when the first thiolization was performed from the liquid phase, which is a direct consequence of capillarity. It was also not observed in our previous work on patterned silane monolayers on silicon, due to the single crystal nature of the Si substrate [4].

A higher friction between the tip and the surface is expected on hydrophilic features [23], which is clearly the case in figure 3(d) (OH-ended nanofeatures in a CH_3-ended background). However, for samples containing small dodecanethiol nanofeatures in an OH-ended background, the friction contrast was frequently reversed compared to this simple expectation. This is for instance the case for the sample displayed in figure 4. This observation indicates that the alkyl-based nanofeatures interact more strongly with the AFM tip than the OH-ended background, which may only be the case if the SAMs in the nanofeatures are of sufficiently high disorder to allow for a higher dissipation of mechanical energy. Indeed, a direct consequence of lower packing density is that a higher friction develops between the tip and the surface [24, 25], as explained above. This observation is in agreement with our previous conclusion that SAM layers grown in the nanoholes of the PMMA mask are of limited quality.

An important parameter of nanopatterned surfaces is their line-edge roughness σ, which is the roughness of the actual contours of the nanofeatures. Since a feature of size lower than about 3σ will not be detectable in the images, the smaller feature achievable by a given lithography method may be taken to be $\sim 3\sigma$. In figure 4(d), the line edges obtained by image discrimination are presented, together with the distribution of local radius from which an rms line-edge roughness of 4.4 nm was obtained. Another independent determination of σ on an array of circles of 70 nm average diameter provided us with a consistent value of 3.2 nm. This indicates that the line-edge roughness is in the range of 4 nm, close to the 3.4 nm previously reported by Stamou *et al* for a similar patterning method of thiol SAMs on gold [7]. The value of $\sim$4 nm found for σ corresponds to a limiting feature size of about 15 nm, in the range of or below the size of most organic macromolecules in solution.

In order to evaluate whether the value found for σ is limited by the lithography method or by an intrinsic physical property of thiol SAMs on gold, we performed a similar evaluation of the line-edge roughness for monolayers of silanes deposited on ultra-flat silicon wafers. The procedure of fabrication of these patterned monolayers is similar to the one used for the thiols, and was reported before [4]. Figure 5 presents an array of $(Cl)_3$–Si–$(CH_2)_6$–COOH dots of 50 nm average diameter, in a background of $Cl(CH_3)_2$–Si–$(CH_2)_2$–$(CF_2)_7$–CF_3. A line-edge roughness of 4 nm is obtained, practically identical to the values obtained for nanopatterned thiol SAMs on gold, indicating that the line-edge roughness is controlled by the lithography process, not by the nature of the substrate and molecules. Considering the potentialities of electron-beam lithography, this observation allows for some room for a further reduction of σ by the proper tuning of lithography parameters. Obviously, other lithographic methods could also be used to define the regions wherein the first thiol monolayer is grown, such as nanoimprint lithography (NIL, which involves the pressing of a hard mold into a polymer mask above its glass transition [26, 27]), or direct writing into a SAM used as resist by electron-beam lithography [28], nanoshaving [29], scanning near-field photolithography [30]

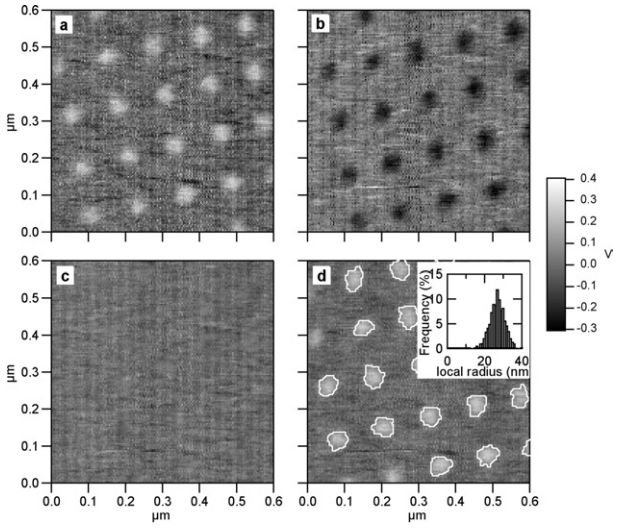

Figure 5. LFM images of a nanopatterned *silane* monolayer on a silicon wafer, where the nanofeatures consist of $(Cl)_3$–Si–$(CH_2)_6$–COOH dots of 50 nm average diameter, in a background of $Cl(CH_3)_2$–Si–$(CH_2)_2$–$(CF_2)_7$–CF_3. ((a), (b)) Trace and retrace LFM images, (c) 'slope' image resulting from the addition of the two LFM images, (d) friction image resulting from the subtraction of the two LFM images. The white contour lines indicate the edges of the two chemical domains, and were used to compute the line-edge roughness, σ. The inset in (d) is the distribution of local radius.

or edge-spreading lithography [31]. Reviews comparing different lithographic methods have been published [20, 32], which should help in selecting a specific lithography for the patterning of SAMs.

Although silane- and thiol-based patterning methods provide identical line-edge roughnesses (∼4 nm) and therefore similar limiting feature sizes (∼15 nm), significant differences nevertheless exist between nanopatterned thiol and silane monolayers. Silane chemistry requires a careful control of humidity in order to get true monolayers reproducibly, whereas thiol chemistry is much easier to perform. However, compared to silanes, thiol monolayers present a series of drawbacks which make them less interesting for nanopatterning applications. First, thiol molecules exchange in solution or in the gas phase [19], which implies the need to strictly control the conditions used during the deposition of the background thiol to avoid scrambling of the patterns (as was done here by working at 5 °C). Second, thiols desorb upon heating even to moderate temperatures [33, 34], which is a significant problem if an annealing step has to be applied at some time during processing. Third, thiols bleed along gold grain boundaries, which tends to blur the nanopatterns. Fourth, the polycrystalline gold substrates used for thiol deposition are intrinsically rougher than the silicon wafers or float glass substrates used for silanes. Finally, gold surfaces are not compatible with many processes used in standard clean rooms, which requires buying expensive dedicated equipment.

Compared to dip pen nanolithography [13], our method has the advantage of being easily scalable to larger surfaces; in addition, by replacing the EBL step by nanoimprint lithography, our method can be strongly accelerated and transformed into a cheap and fully parallel process (contrarily to dip pen or electron-beam nanolithography, which involve serial writing). First attempts to use NIL instead of EBL were performed in our laboratory and elsewhere [11], and provided satisfactory results. However, dip pen nanolithography still appears more appropriate for the formation of nanopatterns involving a large number of different molecules, or for the local deposition of more exotic 'inks' than thiols or silanes.

4. Conclusion

We have shown that 2D chemically nanopatterned gold surfaces can be conveniently produced by combining electron-beam lithography with gas and liquid phase thiolization. The line-edge roughness of the patterns is ∼4 nm, which corresponds to a limiting feature size in the range of 15 nm. These values are close to the ones obtained for silane nanopatterns on silicon, indicating that the limiting step is currently the lithography step, therefore suggesting that improvements in this step may lead to chemical patterns of even higher resolution. Compared to silanes, nanopatterned thiol monolayers suffer from a series of disadvantages, including bleeding of thiols at gold grain boundaries, limited thermal stability and thiol exchange during deposition. Nevertheless, thiols still offer advantages, among which are the large range of available chemical functions for the end groups and their remarkable ease of handling. Such high-resolution patterns may then be used to control the placement of soft molecules at specific locations on hard surfaces, as demonstrated elsewhere [5, 6, 35], thereby paving the way to the integration of the huge library of soft-matter compounds with silicon technology.

Acknowledgments

V Bayot (UCL/DICE), for providing access to EBL facilities, and Anne-Sophie Duwez (UCL/POLY), for helpful discussions about chemical aspects of monolayer formation, are gratefully acknowledged. We are indebted to Professor André Laschewsky and Dr Jörg Bohrisch (Fraunhofer IAP, Potsdam) for providing us with some thiols used at some stages of this work. This research was supported by DG Scientific Research of the French Community of Belgium (Actions de Recherches Concertées 00/05-261 'NANORG'), by the Belgian Science Policy (Interuniversity Attraction Poles) and by the Belgian Fund for Fundamental Collective Research (FRFC). BN is Research Associate of the Belgian National Fund for Scientific Research (FNRS).

References

[1] Craighead H G, Howard R E, Jackel L D and Mankievich P M 1983 *Appl. Phys. Lett.* **42** 38
[2] Chen W and Ahmed H 1993 *Appl. Phys. Lett.* **62** 1499
[3] Vieu C, Carcenac F, Pepin A, Chen Y, Mejias M, Lebib A, Manin-Ferlazzo L, Couraud L and Launois H 2000 *Appl. Surf. Sci.* **164** 111
[4] Pallandre A, Glinel K, Jonas A M and Nysten B 2004 *Nano Lett.* **4** 365

[5] Pallandre A, Moussa A, Nysten B and Jonas A M 2006 *Adv. Mater.* at press
[6] Pallandre A, De Meersman B, Blondeau F, Nysten B and Jonas A M 2005 *J. Am. Chem. Soc.* **127** 4320
[7] Stamou D, Musil C, Ulrich W P, Leufgen K, Padeste C, David C, Gobrecht J, Duschl C and Vogel H 2004 *Langmuir* **20** 3495
[8] Timp G 1999 *Nanotechnology* (New York: Springer)
[9] Ulman A 1999 *Chem. Rev.* **96** 1533
[10] Xia Y, Tien J, Qin D and Whitesides G M 1996 *Langmuir* **12** 4033
[11] Gates B D, Xu Q, Stewart M, Ryan D, Willson C G and Whitesides G M 2005 *Chem. Rev.* **105** 1171
[12] Xu S, Miller S, Laibinis P E and Liu G Y 1999 *Langmuir* **15** 7244
[13] Piner R D, Zhu J, Xu F, Hong S and Mirkin C A 1999 *Science* **283** 661
[14] Eck W, Stadler V, Geyer W, Zharnicow M, Gölzhäuser A and Grunze M 2000 *Adv. Mater.* **12** 805
[15] Gölzhäuser A, Eck W, Geyer W, Stadler V, Weimann T, Hinze P and Grunze M 2001 *Adv. Mater.* **13** 806
[16] Su S, Chong K S L and Leggett G J 2002 *J. Am. Chem. Soc.* **124** 2414
[17] Wagner P, Hoegner M, Güntherodt H J and Semenza G 1995 *Langmuir* **11** 3867
[18] Collard D M and Fox M A 1991 *Langmuir* **7** 1192 and references therein
[19] Baralia G G, Duwez A-S, Nysten B and Jonas A M 2005 *Langmuir* **21** 6825
[20] Campbell S A 2001 *The Science and Engineering of Microelectronic Fabrication* (New York: Oxford University Press) p 343
[21] Schreiber F 2000 *Prog. Surf. Sci.* **65** 151
[22] Bain C D, Troughton E B, Tao Y T, Evall J, Whitesides G M and Nuzzo R G 1989 *J. Am. Chem. Soc.* **111** 321
[23] Beake B D and Leggett G J 2000 *Langmuir* **16** 735
[24] Duwez A S, Jonas U and Klein H 2003 *Chem. Phys. Chem.* **4** 1107
[25] Kim H I, Boiadjiev V, Houston J E, Zhu X Y and Kiely J D 2001 *Tribol. Lett.* **10** 97
[26] Li M, Chen L and Chou S Y 2001 *Appl. Phys. Lett.* **78** 3322
[27] Chou S Y, Krauss P R, Zhang W, Guo L and Zhuang L 1997 *J. Vac. Sci. Technol.* B **15** 2897
[28] Lercel M J, Craighead H G, Parikh A N, Seshadri K and Allara D L 1996 *Appl. Phys. Lett.* **68** 1504
[29] Xu S and Liu G Y 1997 *Langmuir* **13** 127
[30] Sun S and Leggett G J 2004 *Nano Lett.* **4** 1381
[31] Geissler M, McLellan J M, Chen J and Xia Y 2005 *Angew. Chem. Int. Edn* **44** 3596
[32] Gates B D, Xu Q B, Steward M, Ryan D, Willson C G and Whitesides G M 2005 *Chem. Rev.* **105** 1171
[33] Schlenoff J B, Li M and Ly H 1995 *J. Am. Chem. Soc.* **117** 12528
[34] Camillone N, Eisenberger P, Leung T Y B, Schwartz P, Scoles G, Poirier G E and Tarlov M G J 1994 *Chem. Phys.* **101** 11031
[35] Denis F A, Pallandre A, Nysten B, Jonas A M and Dupont-Gillain C 2005 *Small* **1** 984